

---

# Generating images with recurrent adversarial networks

---

**Daniel Jiwoong Im**

Montreal Institute for Learning Algorithms  
University of Montreal  
imdaniel@iro.umontreal.ca

**Chris Dongjoo Kim**

Department of Engineering and Computer Science  
York University  
kimdon20@gmail.com

**Hui Jiang**

Department of Engineering and Computer Science  
York University  
hj@cse.yorku.ca

**Roland Memisevic**

Montreal Institute for Learning Algorithms  
University of Montreal  
memisevr@iro.umontreal.ca

## Abstract

Gatys et al. (2015) showed that optimizing pixels to match features in a convolutional network is a way to render images of high visual quality. Unrolling this gradient-based optimization can be thought of as a recurrent computation, that creates images by incrementally adding onto a visual “canvas”. Inspired by this view we propose a recurrent generative model that can be trained using adversarial training. In order to quantitatively compare adversarial networks we also propose a new performance measure, that is based on letting the generator and discriminator of two models compete against each other.

## 1 Introduction

Generating realistic-looking images has been a long-standing goal in machine learning. The early motivation for generating images was mainly as a diagnostic tool, based on the belief that a good generative model can count as evidence for the degree of “understanding” that a model has of the visual world (see, example, [6], [7], or [16] and references in these). More recently, due to immense quality improvements over the last two years (for example, [5, 1, 15, 2]), and the successes of discriminative modeling overall, image generation has become a goal on its own, with industrial applications within close reach.

Currently, most common image generation models can be roughly categorized into two classes: The first is based on probabilistic generative models, such as the variational autoencoder [11] and a variety of equivalent models introduced at the same time. The idea in these models is to train an autoencoder whose latent representation satisfies certain distributional properties, which makes it easy to sample from the hidden variables, as well as from the data distribution (by plugging samples into the decoder).

The second class of generative models is based on adversarial sampling [4]. This approach forgoes the need to encourage a particular latent distribution (and, in fact, the use of an encoder altogether), by training a simple feed-forward neural network to generate “data-like” examples. “Data-likeness” is judged by a simultaneously trained, but otherwise separate, discriminator neural network.

For both types of approach, sequential variants were introduced recently, which were shown to work much better in terms of visual quality: The DRAW network [5], for example, is a sequential version of the variational autoencoder, where images are generated by accumulating updates into a canvas using a recurrent network. An example of a sequential adversarial network is the LAPGAN model

[1], which generates images in a coarse-to-fine fashion, by generating and upsampling in multiple steps.

Motivated by the successes of sequential generation, in this paper, we propose a new image generation model based on a recurrent network. Similar to [1], our model generates an image in a sequence of structurally identical steps, but in contrast to that work we do not impose a coarse-to-fine (or any other) structure on the generation procedure. Instead we let the recurrent network learn the optimal procedure by itself. In contrast to [5], we obtain very good samples without resorting to an attention mechanism and without variational training criteria (such as a KL-penalty on the hidden).

Our model is mainly inspired by a third type of image generation method proposed recently by [2]. In this work, the goal is to change the texture (or “style”) of a given reference image by generating a new image that matches image features and texture features within the layers of a pretrained convolutional network. As shown by [2], ignoring the style-cost in this approach and only matching image features, it is possible to render images which are similar to the reference image. As we shall show, unrolling the gradient descent based optimization that generates the target image yields a recurrent computation, in which an “encoder” convolutional network extracts images of the current “canvas”. The resulting code and the code for the reference image get fed into a “decoder” which decides on an update to the “canvas”.

This view, along with the successes of trained sequential generation networks, suggests that an iterative convolutional network that is trained to accumulate updates onto a visual canvas should be good at generating images in general, not just those shown as reference images. We show in this paper that this indeed is the case.

To evaluate and compare the relative performance of adversarial generative models quantitatively, we also introduce a new evaluation scheme based on a “cross-over” battle between the discriminators and generators of the two models.

## 2 Background

Generative Adversarial Networks (GAN) are built upon the concept of a non-cooperative game [14], that two networks are trained to play against each other. The two networks are a generative and a discriminative model,  $G$  and  $D$ . The generative model generates samples that are hard for the discriminator  $D$  to distinguish from real data. At the same time, the discriminator tries to avoid getting fooled by the generative model  $G$ .

Formally, the discriminative model is a classifier  $D : \mathbb{R}^M \rightarrow \{0, 1\}$  that tries to determine whether a given point  $\mathbf{x} \in \mathbb{R}^M$  is real or generated data. The generative model  $G : \mathbb{R}^K \rightarrow \mathbb{R}^M$  generates samples  $\mathbf{x} \in \mathbb{R}^M$  that are similar to the data by mapping a sample  $\mathbf{z} \in \mathbb{R}^K$  drawn randomly from some prior distribution  $p(\mathbf{z})$  to the data space. These models can be trained by playing a *minmax game* as follows:

$$\min_{\theta_G} \max_{\theta_D} V(D, G) = \min_G \max_D \left[ \mathbb{E}_{\mathbf{x} \sim p_D} [\log D(\mathbf{x})] + \mathbb{E}_{\mathbf{z} \sim p_G} [\log (1 - D(G(\mathbf{z})))] \right]. \quad (1)$$

where  $\theta_G$  and  $\theta_D$  are the parameters of discriminator and generator, respectively.

In practice, the second term in Equation 1 is troublesome due to the saturation of  $\log(1 - D(G(\mathbf{z})))$ . This makes insufficient gradient flow through the generative model  $G$  as the magnitude of gradients get smaller and prevent them from learning. To remedy the vanishing gradient problem, the objective function in Equation 1 is reformulated into two separate objectives:

$$\max_{\theta_D} \mathbb{E}_{\mathbf{x} \sim p_D} [\log D(\mathbf{x})] + \mathbb{E}_{\mathbf{z} \sim p_G} [\log (1 - D(G(\mathbf{z})))] + \max_{\theta_G} \mathbb{E}_{\mathbf{z} \sim p_G} [\log D(G(\mathbf{z}))]. \quad (2)$$

Although Equation 2 is not the same as Equation 1, the underlying intuition is the same. Moreover, the gradient of generators for the two different objectives are always pointing in the same direction and the two objectives have the same fixed points.

The generating and discriminating procedure are simple. We consider a Gaussian prior distribution with zero-mean and unit variance. Then, the process of generating an output is simply to pass a sample  $\mathbf{z} \sim \mathcal{N}(\boldsymbol{\mu} = \mathbf{0}, \boldsymbol{\sigma} = \mathbf{1})$  to the generative model to obtain the sample  $\mathbf{x} \sim G(\mathbf{z}; \theta_G)$ .

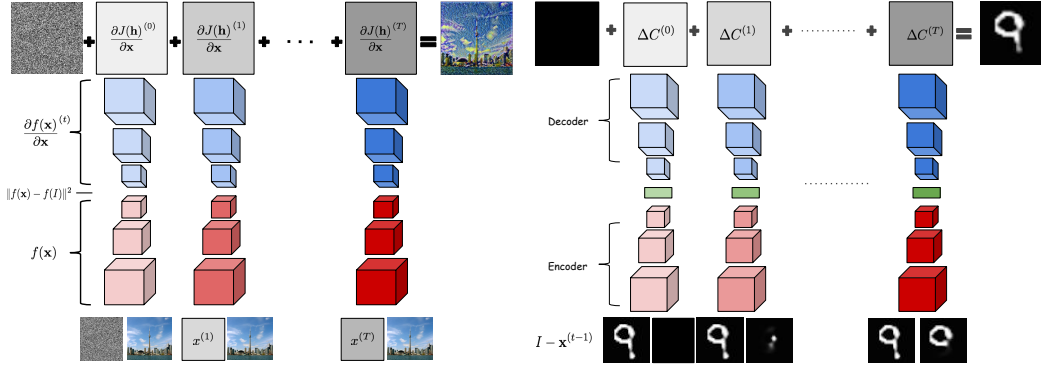


Figure 1: **Left:** Unrolling the gradient-based optimization of pixels in Gatys et al. **Right:** The DRAW network.

Note that the generative model  $G$  can be a deterministic or a probabilistic model. However, only deterministic models have been deployed in the past, so that  $\mathbf{x} = G(\mathbf{z}; \theta_G)$ . Subsequently, the sample can be passed on to the discriminator to predict  $D(\mathbf{x}; \theta_D)$ .

After computing the cost in Equation 2, the model parameters can be updated through backpropagation. Due to the two different min-max operators in Equation 2, the update rule is defined as follows:

$$\{\theta'_D, \theta'_G\} \leftarrow \begin{cases} \text{Update } \theta_D & \text{if } D(\mathbf{x}) \text{ predicts wrong} \\ \text{Update } \theta_D & \text{if } D(G(\mathbf{z})) \text{ predicts wrong} \\ \text{Update } \theta_G & \text{if } D(G(\mathbf{z})) \text{ predicts correct} \end{cases}$$

Ideally, we would like the generative model to learn a distribution such that  $p_G = p_D$ . This requires the generative model to be capable of transforming a simple prior distribution  $p(\mathbf{z})$  to more complex distributions. In general, deep neural networks are good candidates as they are capable of modeling complicated functions and they were shown to be effective in previous works [4, 13, 3, 1].

Recently, [15] showed excellent samples of realistic images using a fully convolutional neural network as the discriminative model and fully deconvolutional neural network [19] as the generative model. The  $l^{\text{th}}$  convolutional layer in the discriminative network takes the form

$$h_j^{k^{(l)}} = f \left( \sum_{j \in M_k} h_j^{l-1} * W^{k^{(l)}} + b_j^{k^{(l)}} \right), \quad (3)$$

and the  $l^{\text{th}}$  convolutional transpose layer<sup>1</sup> in the generative network takes the form

$$g_j^{c^{(l)}} = f \left( \sum_{j \in M_c} g_j^{l-1} \star W^{c^{(l)}} + b_j^{c^{(l)}} \right). \quad (4)$$

In these equations,  $*$  is the convolution operator,  $\star$  is the convolutional transpose operator,  $M_j$  is the selection of inputs from the previous layer (“input maps”),  $f$  is an activation function, and  $\{W^{k^{(l)}}, b_j^{k^{(l)}}\}$  and  $\{W^{c^{(l)}}, b_j^{c^{(l)}}\}$  are the parameters of the discriminator and generator at layer  $l$ . The detailed explanation of convolutional transpose is explained in the supplementary materials.

### 3 Model

We propose sequential modeling using GANs on images. Before introducing our proposed methods, we discuss some of the motivations for our approach. One interesting aspect of models such as the Deep Recurrent Attentive Writer (DRAW) [5] and the Laplacian Generative Adversarial Networks

<sup>1</sup>It is more proper to say “convolutional transpose operation” rather than “deconvolutional” operation. Hence, we will be using the term “convolutional transpose” from now on.

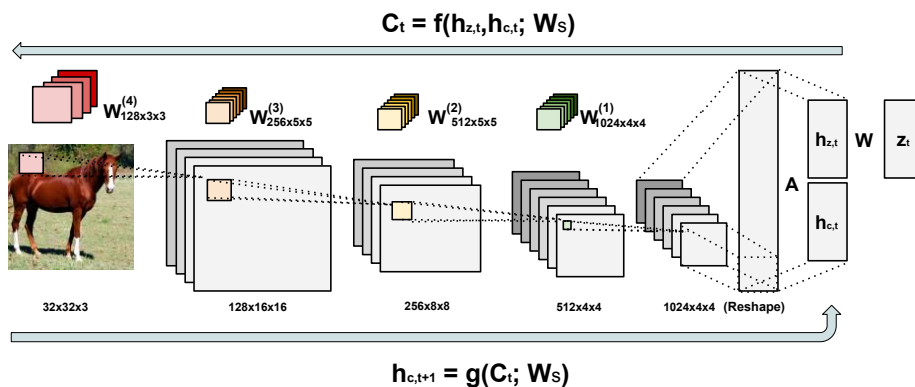


Figure 3: Depiction of single time step component of Generative Recurrent Adversarial Networks architecture layed out. (The numbers of the figures are used for modelling CIFAR10 dataset)

(LAPGAN) [1] is that they generate image samples in a sequential process, rather than generating them in one shot. Both were shown to outperform their ancestor models, which are the variational auto-encoder and GAN, respectively. The obvious advantage of such sequential models is that repeatedly generating outputs conditioned on previous states simplifies the problem of modeling complicated data distributions by mapping them to a sequence of simpler problems.

There is a close relationship between sequential generation and *Backpropagating to the Input* (BI). BI is a well-known technique where the goal is to obtain a neural network *input* that minimizes a given objective function derived from the network. For example, [2] recently introduced a model for stylistic rendering by optimizing the input image to simultaneously match higher-layer features of a *reference content image* and a non-linear, texture-sensitive function of the same features of a *reference style image*. They also showed that in the absence of the style-cost, this optimization yields a rendering of the content image (in a quality that depends on the chosen feature layer).

Interestingly, rendering by feature matching in this way is itself closely related to DRAW: optimizing a matching cost with respect to the input pixels with backprop amounts to first extracting the current image features  $f_x$  at the chosen layer using a forward path through the network (up to that layer). Computing the gradient of the feature reconstruction error then amounts to back-propogating the difference  $f_x - f_I$  back to the pixels. This is equivalent to traversing a “decoder” network, defined as the linearized, inverse network that computes the backward pass. The negative of this derivative is then added into the current version,  $x$ , of the generated image. We can thus think of image  $x$  as a buffer or “canvas” onto which updates are accumulated sequentially (see the left of Figure 2). Like in the DRAW model, where the updates are computed using a (forward) pass through an encoder network, followed by a (backward) pass through a decoder network. This approach is almost identical to the DRAW network, except for two subtle differences (see, [5]): (i) in DRAW, the difference between the current image and the image to be rendered is used in the forward pass, whereas here this difference is computed in the feature space (after encoding); (ii) DRAW uses a learned, attention-based decoder and encoder rather than (fixed) convolutional network. (see the right of Figure 2). We elaborate on the relationship between the two methods in the supplementary material.

In this work, we explore a *generative recurrent adversarial network* as an intermediate between DRAW and gradient-based optimization based on a generative adversarial objective function.

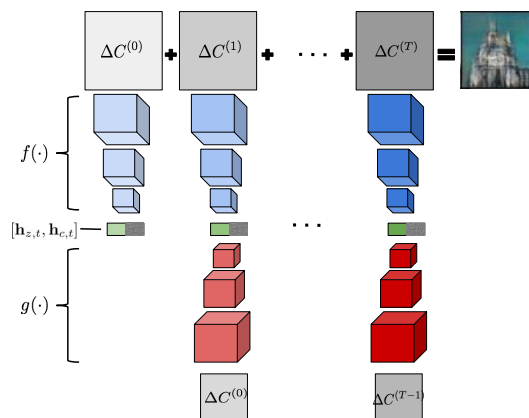


Figure 2: Abstraction of Generative Recurrent Adversarial Networks. The function  $f$  serves as the decoder and the function  $g$  serves as the encoder of GRAN.

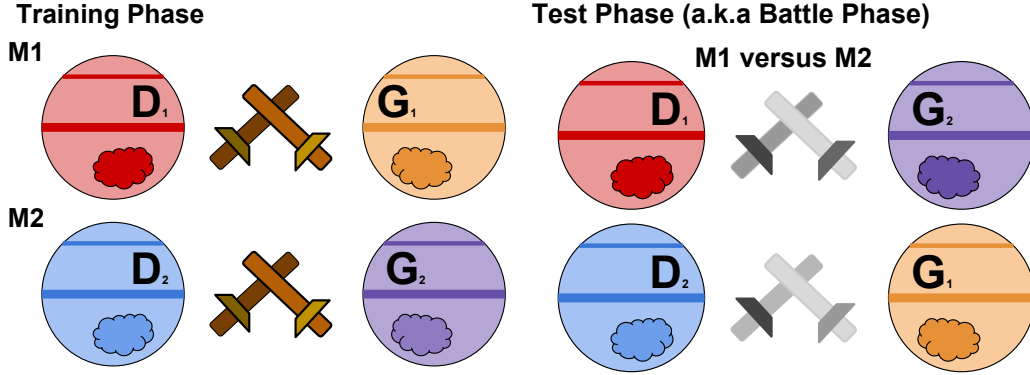


Figure 4: Training Phase of Generative Adversarial Networks. Figure 5: Training Phase and Test Phase of Generative Adversarial Networks.

### 3.1 Generative Recurrent Adversarial Networks

We propose Generative Recurrent Adversarial Networks (GRAN), whose underlying structure is similar to other GANs. The main difference between GRAN versus other generative adversarial models is that the generator  $G$  consists of a recurrent feedback loop that takes a *sequence* of noise samples drawn from the prior distribution  $\mathbf{z} \sim p(\mathbf{z})$  and draws an output at multiple time steps  $\Delta C_1, \Delta C_2, \dots, \Delta C_T$ . Accumulating the updates at each time step yields the final sample drawn to the canvas  $\mathcal{C}$ . Figure 2 delineates the high-level abstraction of GRAN.

At each time step,  $t$ , a sample  $\mathbf{z}$  from the prior distribution is passed to a function  $f(\cdot)$  along with the hidden states  $\mathbf{h}_{c,t}$ . Where  $\mathbf{h}_{c,t}$  represent the hidden state, or in other words, a current encoded status of the previous drawing  $\Delta C_{t-1}$ . Here,  $\Delta C_t$  represents the output of the function  $f(\cdot)$ . (see Supp. Figure 11.) Henceforth, the function  $g(\cdot)$  can be seen as a way to mimic the inverse of the function  $f(\cdot)$ .

Ultimately, the function  $f(\cdot)$  acts as a decoder that receives the input from the previous hidden state  $\mathbf{h}_{c,t}$  and noise sample  $\mathbf{z}$ , and function  $g(\cdot)$  acts as an encoder that provides a hidden representation of the output  $\Delta C_{t-1}$  for time step  $t$ . One interesting aspect of GRAN is that the procedure of GRAN starts with a decoder instead of an encoder. This is in contrast to most auto-encoder like models such as VAE or DRAW, which start by encoding an image (see Figure 2).

In the following, we describe the procedure in more detail. We have an initial hidden state  $\mathbf{h}_{c,0}$  that is set as a zero vector in the beginning. We then compute the following for each time step  $t = 1 \dots T$ :

$$\mathbf{z}_t \sim p(Z) \quad (5)$$

$$\mathbf{h}_{c,t} = g(\Delta C_{t-1}) \quad (6)$$

$$\mathbf{h}_{z,t} = \tanh(W\mathbf{z}_t + \mathbf{b}). \quad (7)$$

$$\Delta C_t = f([\mathbf{h}_{z,t}, \mathbf{h}_{c,t}]), \quad (8)$$

where  $[\mathbf{h}_{z,t}, \mathbf{h}_{c,t}]$  denotes the concatenation of  $\mathbf{h}_{z,t}$  and  $\mathbf{h}_{c,t}$ <sup>2</sup>. Finally, we sum the generated images and apply the logistic function in order to scale the final output to be in  $(0, 1)$ :

$$\mathcal{C} = \sigma\left(\sum_{t=1}^T \Delta C_t\right). \quad (9)$$

The reason for using  $\tanh(\cdot)$  in Equation 7 is to rescale  $\mathbf{z}$  to  $(-1, 1)$ . Hence, rescaling it to the same (bounded) domain as  $\mathbf{h}_{c,t}$ .

In general, one can declare the functions  $f(\cdot)$  and  $g(\cdot)$  to be any type of model. We used a variant of DCGAN [15] in our experiments. Supp. Figure 11 demonstrates the architecture of GRAN at time

<sup>2</sup>Note that we explore two scenarios of sampling  $\mathbf{z}$  in the experiments. The first scenario is where  $\mathbf{z}$  is sampled once in the beginning, then  $\mathbf{h}_{z,t} = \mathbf{h}_z$  as a consequence. In the other scenario,  $\mathbf{z}$  is sampled at every time step.

step  $t$ . The function  $f(\cdot)$  starts with one fully connected layer at the bottom and a deconvolutional layers with fractional-stride convolution at rest of the upper layers. This makes the images gradually upscale as we move up to higher layers. Conversely, the function  $g(\cdot)$  starts from convolutional layers and the fully connected layer at the top. The two functions,  $f(\cdot)$  and  $g(\cdot)$ , are symmetric copies of one another, as shown in Figure 2. The overall network is trained via backpropagation through the time.

## 4 Model Evaluation: Battle between GANs

A problem with generative adversarial models is that there is no obvious way to evaluate them quantitatively. In the past, [4] evaluated GANs by looking at nearest-neighbours in the training data. LAPGAN was evaluated in the same way, and in addition using human inspections [1]. For these, volunteers were asked to judge whether given images are drawn from the dataset or generated by LAPGAN. In that case, the human acts as the discriminator, while the generator is a trained GAN. The problem with this approach is that human inspectors can be subjective to high variance, which makes it necessary to average over a large number of these, and the experimental setup is expensive and cumbersome. A third evaluation scheme, used recently by [15] is based on classification performance. However, this approach is rather indirect and relies heavily on the choice of classifier. For example, in the work by Radford et al, they used nearest neighbor classifiers, which suffers from the problem that Euclidean distance is not a good dissimilarity measure for images.

Here, we propose an alternative way to evaluate generative adversarial models. Our approach is to directly compare two generative adversarial models by having them engage in a ‘‘battle’’ against each other. The naive intuition is that, since every generative adversarial models consists of a discriminator and a generator in pairs, we can exchange the pairs and have the models play the generative adversarial game against each other. Figure 5 illustrates this approach<sup>3</sup>.

The training and test stages are as follows. Consider two generative adversarial models,  $M_1$  and  $M_2$ . Each model consists of a generator and a discriminator,  $M_1 = \{(G_1, D_1)\}$  and  $M_2 = \{(G_2, D_2)\}$ . In the training phase,  $G_1$  competes with  $D_1$  in order to be trained for the battle in the test phase. Likewise for  $G_2$  and  $D_2$ . In the test phase, model  $M_1$  plays against model  $M_2$  by having  $G_1$  try to fool  $D_2$  and vice-versa.

Figure 6: Model Comparison Metric for GANs

	$M_1$	$M_2$
$M_1$	$D_1(G_1(\mathbf{z})), D_1(\mathbf{x}_{train})$	$D_1(G_2(\mathbf{z})), D_1(\mathbf{x}_{test})$
$M_2$	$D_2(G_1(\mathbf{z})), D_2(\mathbf{x}_{test})$	$D_2(G_2(\mathbf{z})), D_2(\mathbf{x}_{train})$

Accordingly, we end up with the combinations shown in Table 6. Each entry in the table contains two scores, one from discriminating training or test

data points, and the other from discriminating generated samples. At test time, we can look at the following ratios between the discriminative scores of the two models:

$$r_{test} \stackrel{\text{def}}{=} \frac{\epsilon(D_1(\mathbf{x}_{test}))}{\epsilon(D_2(\mathbf{x}_{test}))} \text{ and } r_{sample} \stackrel{\text{def}}{=} \frac{\epsilon(D_1(G_2(\mathbf{z})))}{\epsilon(D_2(G_1(\mathbf{z})))}, \quad (10)$$

where  $\epsilon(\cdot)$  is the classification error rate, and  $x_{test}$  is the predefined test set. These ratios allow us to compare the model performances.

The test ratio,  $r_{test}$ , tells us which model generalizes better since it is based on discriminating the test data. Note that when the discriminator is overfitted to the training data, the generator will also be affected by this. This will increase the chance of producing biased samples towards the training data.

The sample ratio,  $r_{sample}$ , tells us which model can fool the other model more easily, since the discriminators are classifying over the samples generated by their opponents. Strictly speaking, as our goal is to generate good samples, the sample ratio determines which model is better at generating good (‘‘data like’’) samples.

We suggest using the sample ratio to determine the winning model, and to use the test ratio to determine the validity of the outcome. The reason for using the latter is due to the occasional possibility of the sample ratio being biased, in which case the battle is not completely fair when

<sup>3</sup>A larger figure is shown in the supplementary materials.

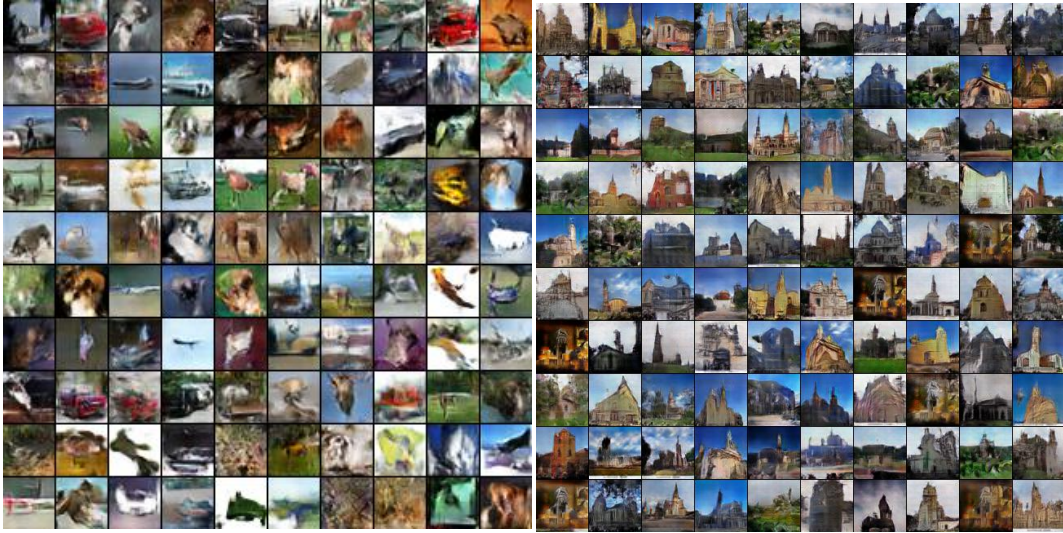


Figure 7: Cifar10 samples generated by GRAN      Figure 8: LSUN samples generated by GRAN

Table 1: Model Evaluation on various data sets.

Data set	Battler	$r_{test}$	$r_{sample}$	Winner
MNIST	GRAN1 vs. GRAN3	0.79	1.75	GRAN3
	GRAN1 vs. GRAN5	0.95	1.19	GRAN5
CIFAR10	GRAN1 vs. GRAN3	1.28	1.001	GRAN3
	GRAN1 vs. GRAN5	1.29	1.011	GRAN5
	GRAN3 vs. GRAN5	1.00	2.289	GRAN5
LSUN	GRAN1 vs. GRAN3	0.95	13.68	GRAN3
	GRAN1 vs. GRAN5	0.99	13.97	GRAN5
	GRAN3 vs. GRAN5	0.99	2.38	GRAN5

Table 2: Comparison between GRAN and non-adversarial models on MNIST.

Battler	Error
GRAN1 vs. DVAE	0.058
GRAN3 vs. DVAE	0.01
GRAN1 vs. DRAW	0.347
GRAN3 vs. DRAW	0.106

the winner is solely determined by the sample ratio. It is possible that one of the discriminators is biased towards the training data more so than the other (i.e. overfitted on the training data). In order to address this issue, our proposed evaluation metric qualifies the sample ratio to be judged by the test ratio as follows:

$$\text{winner} = \begin{cases} \text{M1} & \text{if } r_{sample} < 1 \text{ and } r_{test} \simeq 1 \\ \text{M2} & \text{if } r_{sample} > 1 \text{ and } r_{test} \simeq 1 \\ \text{Tie} & \text{otherwise} \end{cases} \quad (11)$$

This imposes a condition where  $r_{test} \simeq 1$ , which assures that none of the discriminator is overfitted more than the other. If  $r_{test} \neq 1$ , then this implies that  $r_{sample}$  is biased, and thus, the sample ratio is no longer applicable.

We call this evaluation measure Generative Adversarial Metric (GAM). GAM is not only able to compare generative adversarial models against each other, but also able to partially compare other models, such as the VAE or DRAW. This is done by observing the error rate of GRAN’s discriminators based on the samples of the other generative model as an evaluation criterion. For example, in our experiments we report the error rates of the GRAN’s discriminators with the samples of other generative models, i.e.  $err(D(\mathbf{z}))$  where  $\mathbf{z}$  are the samples of other generative models and  $D(\cdot)$  is the discriminator of GRAN.

## 5 Experiments

In order to evaluate whether the extension of sequential generation enhances the performance, we assessed both quantitatively and qualitatively under three different image datasets. We conducted several empirical studies on GRAN under the model selection metrics discussed in Section 4. See Supplementary Materials for full experimental details.

The performance of GRAN is presented in Table 1. We focused on comparing GRANs with 1, 3 and 5 time steps. For all three datasets, GRAN3 and GRAN5 outperformed GRAN1 as shown in

Table 1. Moreover, we present samples from GRAN for MNIST, cifar10 and LSUN in Figure 7, Figure 8, and Supp. Figure 12. Most of the MNIST and cifar10 samples shown in Supp. Figure 12 and Figure 7 appear to be discernible and reasonably classifiable by humans. Additionally, the LSUN samples from Figure 8 seem to cover variety of church buildings and contain fine detailed textures. The “image statistics” of two real image datasets are embedded into both types of sample.

In the following, we analyze the results by answering a set of questions on our experiments.

*Q: How do GRAN and other GAN type of models perform compared to non generative adversarial models?*

We compared our model to other generative models such as denoising VAE (DVAE) [8] and DRAW on the MNIST dataset. Although this may not be the best way to assess the two models, since the generator of GRAN is not used, Table 2 presents the results of applying GAM as described at the end of Section 4. The error rates were all below 50%, and especially low for DVAE’s samples. Surprisingly, even though samples from DRAW look very nice, the error rate on their samples were also quite low with GRAN3. This illustrates that the discriminators of generative adversarial models are good at discriminating the samples generated by DVAE and DRAW. Our hypothesis is that the samples look nicer due to the smoothing effect of having a mean squared error in their objective, but they do not capture all relevant aspects of the statistics of real handwritten images.



Figure 9: Nearest Neighbour training examples for cifar10 samples.

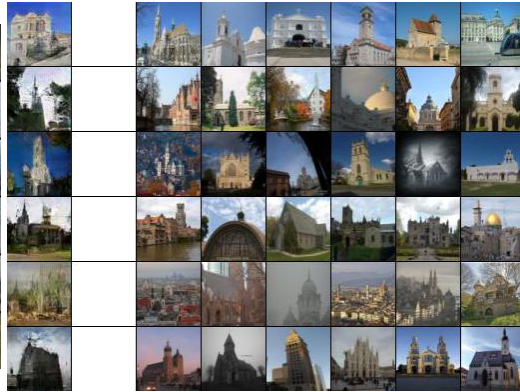


Figure 10: Nearest Neighbour training examples for lsun samples using GRAN3.

*Q: Does GRAN overfit to the training data?*

Since it is infeasible to naively examine the training data for similar looking images as GRAN’s output, it is common (albeit somewhat questionable) to look at  $k$ -nearest neighbors to do a basic sanity check. As shown in Supp. Figure 13, Supp. Figure 16, and Supp. Figure 17 and 18, one does not find any replicates of training data cases.

Empirically speaking, we did notice that GRAN tends to generate samples by interpolating between the training data. For example, Supp. Figure 11 illustrates that the church buildings consist of similar structure of the entrance but the overall structure of the church has a different shape. Based on such examples, we hypothesize that the overfitting for GRAN in the worst case may imply that the model learns to interpolate sensibly between training examples. This is not the typical way of the term overfitting is used for generative models, which usually refers to memorizing the data. In fact, in adversarial training in general, the objective function is not based on mean squared error of the pixels which makes it not obvious how to memorize the training samples. However, this could mean that it is difficult for these models to generate images that are interpolated from training data.



Figure 11: Drawing at different time steps on cifar10 samples.



Figure 12: Drawing at different time steps on lsun samples.



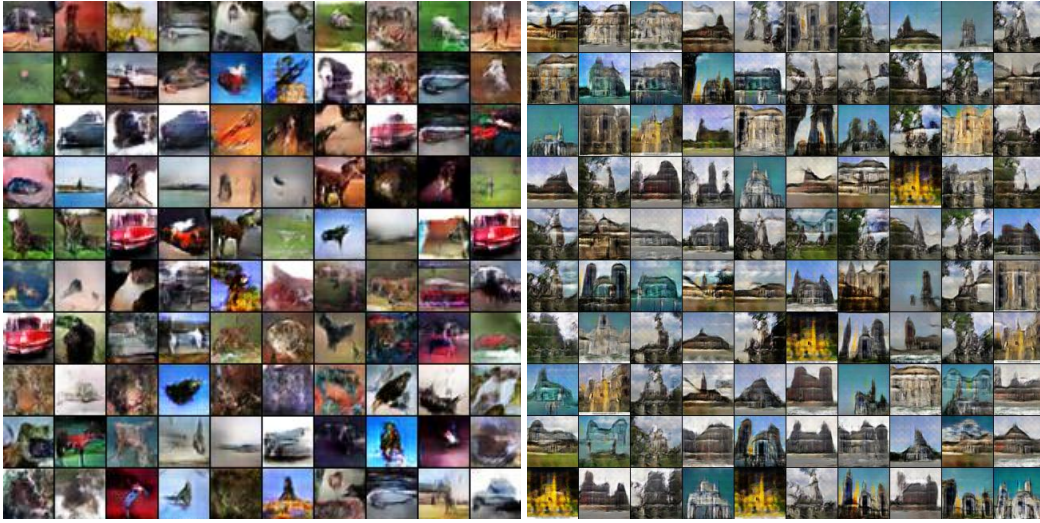


Figure 13: Cifar10 samples generated by GRAN with injecting different noises at every time step Figure 14: LSUN samples generated by GRAN with injecting different noises at every time step

*Q: What do the samples look during the intermediate time steps?*

Supp. Figure 14, Supp. Figure 21, and Supp. Figure 22 present the intermediate samples when the total number of steps is 3. From the figures, we can observe the gradual development of the samples over time. The common observation from the intermediate samples is that images become more fine-grained and introduce details missing from the previous time step image. Intermediate samples for models with a total number of time steps of 5 can be found in the supplementary materials as well. This behaviour is somewhat similar to [1], as one might expect (although filling-in of color details suggest that the process is more complex than a simple coarse-to-fine generation). Note that this behaviour is not enforced in our case, since we use an identical architecture at every time step.

*Q: What happens when we use a different noises for each step?*

We sampled a noise vector  $\mathbf{z} \sim p(Z)$  and used the same noise for every time step. This is because  $\mathbf{z}$  acts as a reference frame in [2] as shown in Figure 2. On the other hand, the role of the sample in DRAW is to inject noise at each step,  $\mathbf{z}_1, \mathbf{z}_2, \dots, \mathbf{z}_T, \sim p(Z)$ , as prescribed by the variational auto-encoding framework. We also experimented with both sampling  $\mathbf{z}$  once in the beginning versus sampling  $\mathbf{z}_i$  at each time step. Here we describe the advantages and disadvantages to these two approaches.

The samples of cifar10 and LSUN generated by injecting different noises at each time step are shown in Supp. Figure 19 and Supp. Figure 20. Figure 7 and Figure 8 are the output samples when injected using the same noise. The samples appear to be discernible and reasonably classifiable by humans as well. However, we observe a few samples that look very alike to one other. During the experiments, we found that when using different noise, it requires more effort to find a set of hyper-parameters that produce good samples. Furthermore, the samples tend to collapse when training for a long time. Hence, we had to carefully select the total number of iterations. This illustrates that the training became much more difficult and it provokes GRAN to “cheat” by putting a lot of probability mass on samples that the discriminator cannot classify, which produce samples that look very similar to each other.

On the other hand, when we look at the intermediate time steps of samples generated using multiple noises, we find that there are more pronounced changes within each time step as demonstrated in Supp. Figure 19 and Supp. Figure 20. For example, the colour of the train in Supp. Figure 19 changes, and a partial church is drawn in Supp. Figure 20.

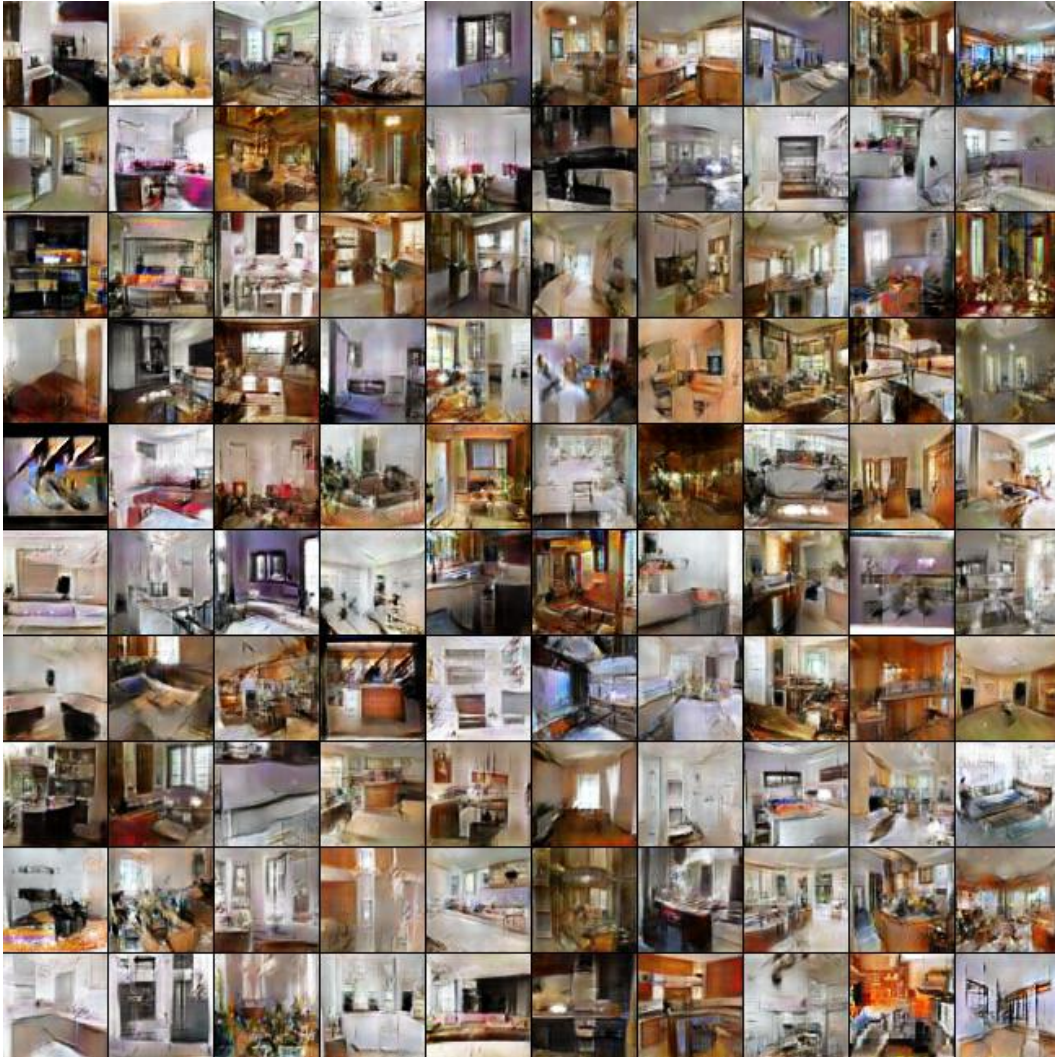


Figure 15: LSUN (living room +kitchen) samples generated by GRAN3.

## 6 Conclusion

We proposed a new generative model based on adversarial training of a recurrent neural network inspired by [2]. We showed the conditions under which the model performs well and also showed that it can produce higher quality visual samples than an equivalent single-step model. We also introduced a new metric for comparing adversarial networks quantitatively and presented that the recurrent generative model yields a superior performance over existing state-of-the-art generative models under this metric.

## Acknowledgements

We thank the members of the LISA Lab at Montreal, in particular Mohammed Pezeshki and Donghyun Lee, for helpful discussions.

This research was developed with funding from the Defense Advanced Research Projects Agency (DARPA). The views, opinions, and/or findings expressed are those of the author and should not be interpreted as representing the official views or policies of the Department of Defense or the U.S. Government.

## References

- [1] Emily Denton, Soumith Chintala, Arthur Szlam, and Rob Fergus. Deep generative image models using a laplacian pyramid of adversarial networks. In *Proceedings of the Neural Information Processing Systems (NIPS)*, 2015.
- [2] Leon A Gatys, Alexander S Ecker, and Matthias Bethge. A neural algorithm of artistic style. *arXiv preprint arXiv:1508.06576*, 2015.
- [3] Jon Gauthier. Conditional generative adversarial nets for convolutional face generation. In *Class Project for Stanford CS231N: Convolutional Neural Networks for Visual Recognition, Winter semester 2014*, 2014.
- [4] Ian J. Goodfellow, Jean Pouget-Abadie, Mehdi Mirza, Bing Xu, David Warde-Farley, Sherjil Ozair, Aaron Courville, and Yoshua Bengio. Generative adversarial nets. In *Proceedings of the Neural Information Processing Systems (NIPS)*, 2014.
- [5] Karol Gregor, Ivo Danihelka, Alex Graves, Danilo Jimenez Rezende, and Daan Wierstra. Draw: A recurrent neural network for image generation. In *Proceedings of the International Conference on Machine Learning (ICML)*, 2015.
- [6] Geoffrey E. Hinton, Simon Osindero, and Yee-Whye Teh. A fast learning algorithm for deep belief nets. *Neural Computation*, 18(7):1527–1554, 2006.
- [7] Aapo Hyvriinen, Jarmo Hurri, and Patrick O. Hoyer. *Natural Image Statistics: A Probabilistic Approach to Early Computational Vision*. Springer Publishing Company, Incorporated, 1st edition, 2009.
- [8] Daniel Jiwoong Im, Sungjin Ahn, Roland Memisevic, and Yoshua Bengio. Denoising criterion for variational auto-encoding framework. In <http://arxiv.org/abs/1511.06406>, 2015.
- [9] Sergey Ioffe and Christian Szegedy. Batch normalization: Accelerating deep network training by reducing internal covariate shift. In <http://arxiv.org/pdf/1502.03167.pdf>, 2015.
- [10] Diederik Kingma and Jimmy Ba. Adam: A method for stochastic optimization. In *Proceedings of the International Conference on Learning Representations (ICLR)*, 2014.
- [11] Diederik P Kingma and Max Welling. Auto-encoding variational bayes. In *Proceedings of the Neural Information Processing Systems (NIPS)*, 2014.
- [12] Andrew L Maas, Awni Y Hannun, and Andrew Y. Ng. Rectifier nonlinearities improve neural network acoustic models. In *Proceedings of the International Conference on Machine Learning (ICML)*, 2013.
- [13] Mehdi Mirza and Simon Osindero. Conditional generative adversarial nets. In *Proceedings of the Neural Information Processing Systems Deep learning Workshop(NIPS)*, 2014.
- [14] John Nash. Non-cooperative games. *The Annals of Mathematics*, 54(2):286–295, 1951.
- [15] Alec Radford, Luke Metz, and Soumith Chintala. Unsupervised representation learning with deep convolutional generative adversarial networks. In *Proceedings of the International Conference on Learning Representations (ICLR)*, 2015.
- [16] Marc’Aurelio Ranzato, Volodymyr Mnih, Joshua M Susskind, and Geoffrey E Hinton. Modeling natural images using gated mrfs. *Pattern Analysis and Machine Intelligence, IEEE Transactions on*, 35(9):2206–2222, 2013.
- [17] Jost Tobias Springenberg, Alexey Dosovitskiy, Thomas Brox, and Martin. Riedmiller. Striving for simplicity: The all convolutional net. In <http://arxiv.org/abs/1412.6806>, 2014.
- [18] Fisher Yu, Yinda Zhang, Shuran Song, Ari Seff, and Jianxiong Xiao. Lsun: Construction of a large-scale image dataset using deep learning with humans in the loop. In *arXiv:1506.03365 [cs.CV] 10 Jun 2015*, 2015.
- [19] Matthew D. Zeiler, Graham W. Taylor, and Rob Fergus. Adaptive deconvolutional networks for mid and high level feature learning. In *International Conference on Computer Visio*, 2011.

## Supplementary Materials

### Additional Notes on Convolutional Transpose

In the following, we describe the convolutional transpose procedure in detail. For simplicity, let us consider the case of a 1-dimensional convolutional operation with one kernel and stride of 1:

$$o = i * W, \quad (12)$$

where  $i$  is an input,  $o$  is an output, and  $*$  is the convolutional operator. Figure 16 and Figure 17 show an illustration of the 1D convolution.

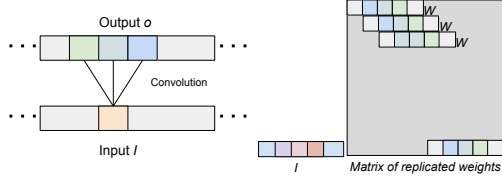


Figure 18: The gradient of convolution at index  $k$ .

Figure 19: Convolution operation as a matrix operations.

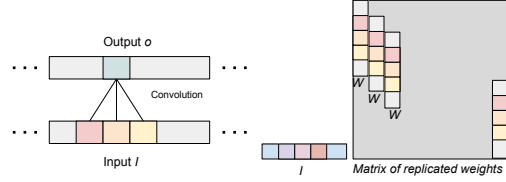


Figure 16: Applying Figure 17: Convolution convolution at index  $j$ . operation as a matrix operation.

Figure 16 presents the naive visualization of convolution over the input centered at index  $j$ , and Figure 17 presents the convolution operation in terms of matrix operation. The latter figure will be useful for understanding the convolutional transpose.

The gradient of Equation 15 wrt. the input takes the form

$$\frac{\partial o}{\partial i} = \frac{\partial i * W}{\partial i}. \quad (13)$$

Note that gradient of the convolution is a convolution itself. This can be seen in Figure 18. We can re-express the *convolutional transpose*

$$\tilde{o} = \tilde{i} \star W \quad (14)$$

where  $\star$  is a convolutional transpose operator, and  $\tilde{o}$  and  $\tilde{i}$  are just input and output of the function.

From Figure 19, we can observe that the gradient of convolutional formula in Equation 15 is just a transpose of the replicated input matrix. Since the convolutional gradient uses the convolutional transpose operator, the convolutional transpose can be implemented by using the gradient.

Now we consider the case of strided convolution. For simplicity, we assume that the stride is 2. Similarly to before, we can write

$$o = i * W, \quad (15)$$

where  $i$  is an input,  $o$  is an output, and  $*$  is the convolution operator. Figure 20 and Figure 21 illustrate the 1D convolution.

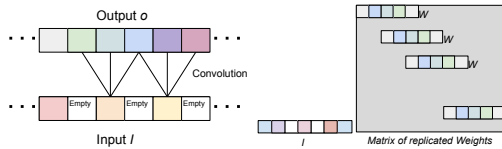


Figure 22: The gradient of convolution at index  $k$ .

Figure 23: Convolution operation as a matrix operations.

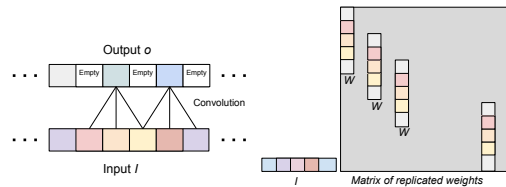


Figure 20: Applying Figure 21: Stride Convolution convolution at index  $j$ . operation as a matrix operations.

Figure 20 shows the visualization of 2-stride convolution over the input centered at index  $j$  and Figure 17 presents stride convolution operation in terms of a matrix operation.

The gradient of Equation 15 takes the form

$$\frac{\partial o}{\partial \hat{i}} = \frac{\partial \hat{i} * W}{\partial \hat{i}}. \quad (16)$$

where  $\hat{i}$  is the upsampled input  $i$  such that  $\hat{i} = [i_1, 0, i_2, 0, i_3, \dots, i_M, 0]$  for stride size equal to

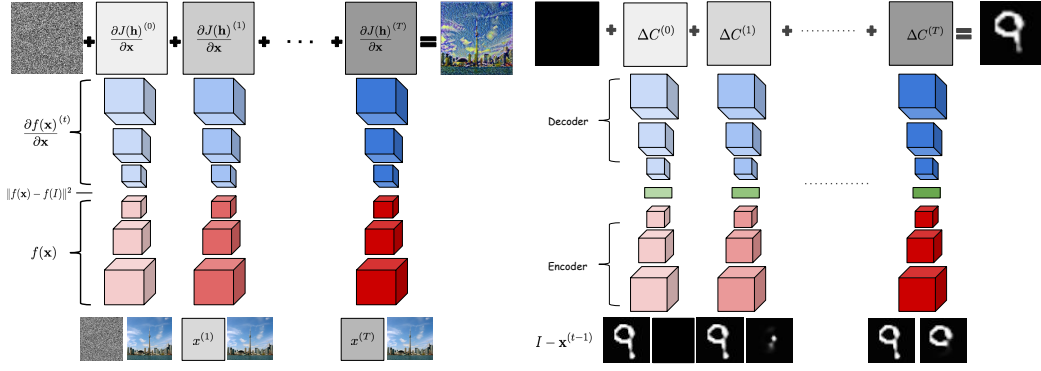


Figure 24: The gradient of convolution at index  $k$ . Figure 25: The abstract view of DRAW architecture is delineated.

2. Thus, the gradient of the strided convolution is a convolutional operation on an upsampled version of the input  $i$ . This can be observed from Figure 22.

Overall, the convolutional transpose with strides is expressed as

$$\hat{o} = \hat{i} \star W \quad (17)$$

where  $\star$  is a convolutional transpose operator, and  $\hat{o}$  and  $\hat{i}$  are just input and output of the function.

### Relation between sequential modeling and backpropagation with respect to the input methods

We describe in more detail the relation between sequential modeling algorithms and backpropagation with respect to the input (BI). We will investigate their relation by examining a specific example.

The goal of BI is to find an optimal input by backpropagating an objective function with respect to the input. Let  $J(\mathbf{x})$  be a differentiable objective function that takes an input  $\mathbf{x}$ . Then, depending on whether the objective function is non-linear function or not, we iterate

$$x_{opt} = x^{(0)} - \sum_{t=1}^T \eta_t \frac{\partial J^{(t)}}{\partial \mathbf{x}^{(t-1)}} \quad (18)$$

where  $t$  denotes time, and the chain rule yields

$$\frac{\partial J^{(t)}}{\partial \mathbf{x}^{(t-1)}} = \frac{\partial J^{(t)}}{\partial f^{(t)}} \frac{\partial f^{(t)}}{\partial \mathbf{x}^{(t-1)}}, \quad (19)$$

where  $f(\cdot)$  is an intermediate function, which can be composed of many non-linear functions like neural networks, in the objective function  $J(\cdot)$ .

An example method that uses backpropagation with respect to the input is [2]. We will consider with only the content based objective of this method, and compare it to one of the well-known sequential generators, DRAW [5]. Figure 24 presents unrolled version. The objective function of BI is defined as  $\|f_{\mathbf{x}} - f_I\|^2$  where  $f_{\mathbf{x}}$  is the hidden representation of the input  $\mathbf{x}^{(t)}$ , and  $h_I$  is the hidden representation of the *reference content image* of the convolutional network  $f(\cdot)$ . The network layers are shown as red blocks. Furthermore, the blue blocks (or the upper half) the diagram in Figure 24 is the unrolled part of backpropagation gradient with respect to the input  $\frac{\partial f}{\partial \mathbf{x}}$ .

The architecture of DRAW is shown in Figure 25<sup>4</sup>. DRAW takes the input and the difference between the input and canvas at time  $t$ , and it propagates through the encoder and decoder. At the end of each time step, DRAW outputs the updated canvas  $C^{(t)}$  by updating the previous canvas  $C^{(t-1)}$  with what will be drawn at time  $t$ , which is equivalent to change in the canvas  $\Delta C^{(t)}$ .

<sup>4</sup>The attention mechanism is omitted for clarity.

We can immediately notice the similarity between two architectures. The update procedure of draw, which is expressed as

$$C^{(t)} = C^{(t-1)} + \Delta C^{(t)}, \quad (20)$$

resembles the update rule of BI in Equation 18. Moreover, the encoder of DRAW,  $enc(\cdot)$ , can be seen as some function  $f(\cdot)$ , which will be the convolutional neural network in BI. Similarly, the decoder of DRAW,  $dec(\cdot)$ , can be seen as the unrolled version of BI, which corresponds to  $\frac{\partial f^{(t)}}{\partial \mathbf{x}^{(t-1)}}$ . The main difference is that BI takes the difference in the hidden representation space of  $f(\cdot)$  and DRAW takes the difference from the original input space.

Overall, we linked each components of two models by examining the abstraction as shown:

- $\Delta C^{(t)}$  reflects  $\frac{\partial J^{(t)}}{\partial \mathbf{x}^{(t-1)}}$ .
- $enc(\cdot)$  and  $dec(\cdot)$  reflect  $f(\cdot)$  and  $\frac{\partial f^{(t)}}{\partial \mathbf{x}^{(t-1)}}$ .

### Supplementary Material to the Experiments

**The MNIST dataset** contains 60,000 images for training and 10,000 images for testing and each of the images is  $28 \times 28$  pixels for handwritten digits from 0 to 9 (LeCun et al., 1998). Out of the 60,000 training examples, we used 10,000 examples as validation set to tune the hyper-parameters of our model.

**The CIFAR10 dataset** consists of 60000  $32 \times 32$  colour images in 10 classes, with 6000 images per class. There are 50000 training images and 10000 test images.

**The LSUN Church dataset** consists of high resolution natural scene images with 10 different classes [18]. We considered training on outdoor church images, which contains 126,227 training, 300 validation, and 1000 test images. These images were downsampled to  $64 \times 64$  pixels.

**The LSUN Living Room + Kitchen dataset** consists of high resolution natural scene images with 10 different classes [18]. We considered training on living room and kitchen images, which contains approx. 120,000 training, 300 validation, and 1000 test images. These images were downsampled to  $64 \times 64$  pixels.

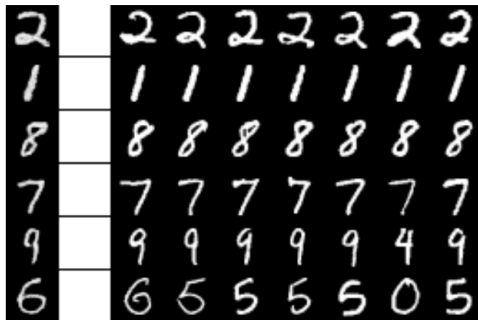


Figure 27: Nearest Neighbour training examples for MNIST samples.



Figure 28: Drawing at different time steps on mnist samples.

---

### Algorithm 1 GRAN's sample generating process.

---

Initial hidden state:  $\mathbf{h}_{c,0} = \mathbf{0}$ .

```

while  $t < T$  do
   $\mathbf{z}_t \sim p(Z)$ 
   $\mathbf{h}_z = \tanh(W\mathbf{z}_t + \mathbf{b})$ 
   $\mathbf{h}_{c,t} = g(\Delta C_{t-1})$ 
   $\Delta C_t = f([\mathbf{h}_z, \mathbf{h}_{c,t}])$ 
end while
 $C = \sigma(\sum_{t=1}^T \Delta C_t)$ 

```

---



Figure 26: MNIST Samples generated by GRAN

All datasets were normalized such that each pixel value ranges in between  $[0, 1]$ . For all of our results, we optimized the models with ADAM [10]. The batch size was set to 100, and the learning rate was selected from a discrete range chosen based on the validation set. Importantly, we used different learning rates for the discriminative network and generative network. Throughout the experiments, we found that having different learning rates are useful to obtain successfully trained generative adversarial models. As our proposed model is a sequential generator, we must select the number of steps,  $T$ , to run the model for generation. We compared the models in different number of timesteps,  $\{1, 3, 5\}$ . Note that GRAN is equivalent to DCGAN when  $T = 1$  up to one extra fully connected layer. We denote this as GRAN1.

Throughout the experiments, we used a similar architecture for the generative and discriminative network as shown in Figure 3 and Figure 2.

Figure 29: The experimental hyper-parameters on different data sets.

DATASET	# KERNELS	FILTER SZ.	# $\mathbf{z}$
MNIST	[80, 40, 1]	[5,5,5]	60
CIFAR10	[1024, 512, 216, 3]	[5,5,5,5]	100
LSUN	[1024, 512, 216, 128, 3]	[5,5,5,5,5]	100

The convolutional layers of the networks for the discriminator and generator are shared. The number of convolutional layers and the number of hidden units at each layer were varied based on the dataset. Table 29 shows the number of convolution kernels and the size of the filters at each convolutional layer. The numbers in the array from left to right corresponds to each bottom to top layer of the convolutional neural network. One can tie the weights of convolution and convolutional transpose in the encoder and decoder of GRAN to have the same number of parameters for both DCGAN and GRAN.

The quality of samples can depend on several tricks [15], including:

1. Removing fully connected hidden layers and replacing pooling layers with strided convolutions on the discriminator [17] and fractional-strided convolutions (upsampling) on the generator.
2. Using batch-normalization [9] on both generative and discriminative models.
3. Using ReLU activations in every layer of the generative model except the last layer, and using LeakyReLU activations [12] in all layers of the discriminative model.

Overall, these architectural tricks make it easier to generate smooth and realistic samples. We rely on these tricks and incorporate them into GRAN.

**Analysis on GRAN samples** The following figure is to support the studies in the experiments, particularly it supports the description under  $Q$ : *Does GRAN overfit the training data?*



Figure 30: Example of three different churches (samples) with some similarities.

**Nearest Neighbours of samples from the training dataset**

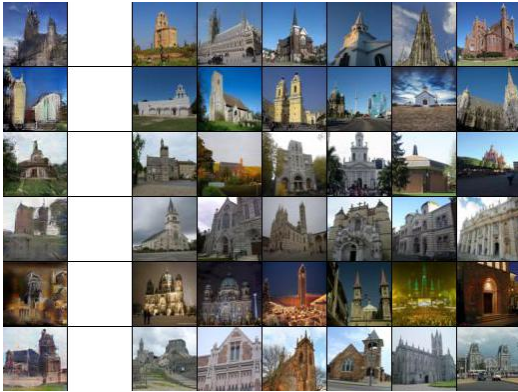


Figure 31: Nearest Neighbour training examples for lsun church samples using GRAN5.



Figure 32: Nearest Neighbour training examples for lsun (living room + kitchen) samples.

**Intermediate samples at time step for GRAN5**

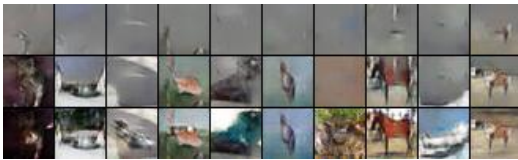


Figure 33: Drawing at different time steps on ci-far10 samples with injecting different noises at every time step.

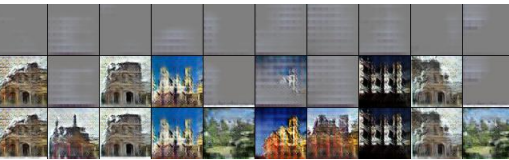


Figure 34: Drawing at different time steps on lsun samples with injecting different noises at every time step.



Figure 35: Drawing at different time steps on ci-far10 samples.



Figure 36: Drawing at different time steps on lsun church samples.



Figure 37: Drawing at different time steps on lsun (living room + kitchen) samples.





Figure 38: LSUN (church) samples generated by GRAN5.

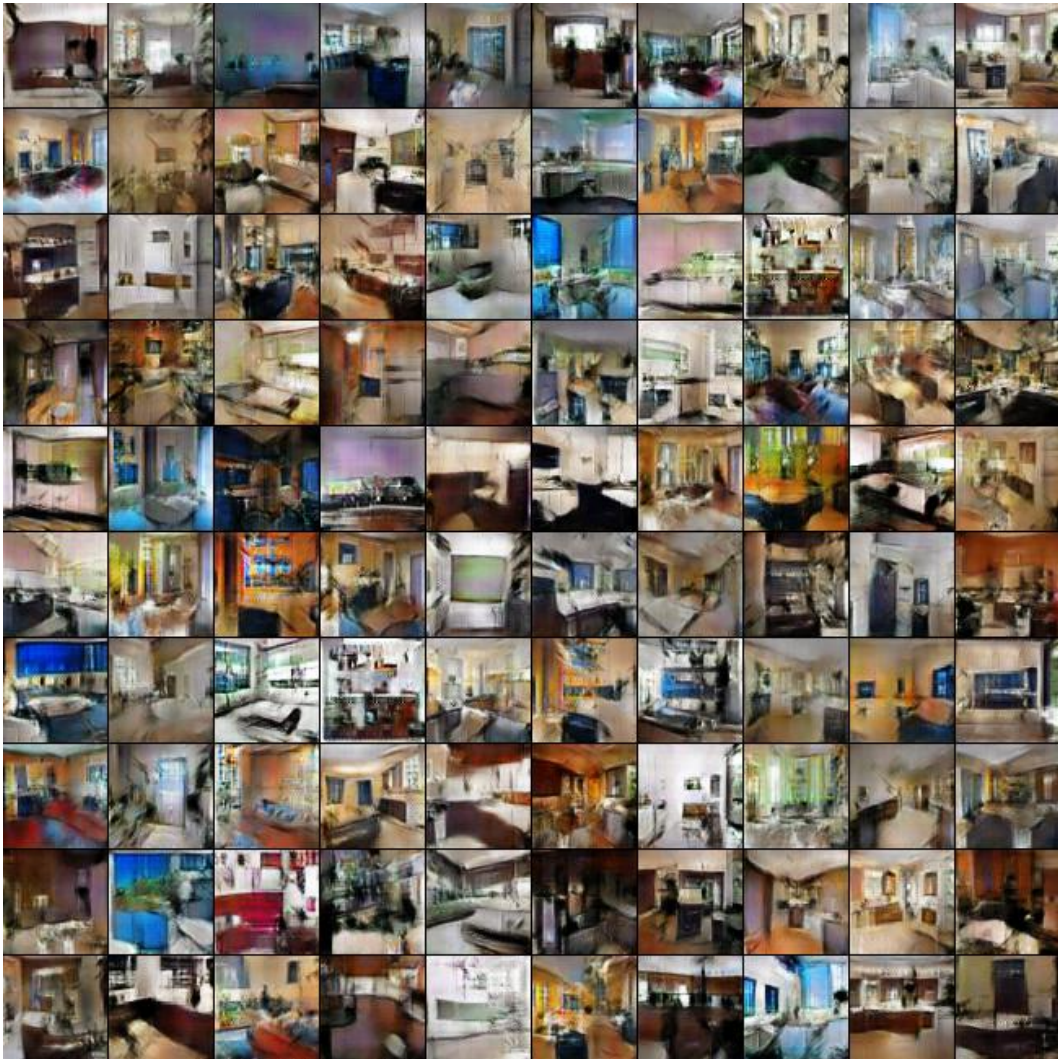


Figure 39: LSUN (living room +kitchen) samples generated by GRAN5.

### ImageNet samples

We also trained GRAN on ImageNet dataset. ImageNet dataset (Deng et al., 2009) is a high resolution natural images. We rescaled the images to  $64 \times 64$  pixels. The architecture that was used for ImageNet is same as the architecture that was used for LSUN dataset except that there are three times more kernels on both generator and discriminator.

The samples are shown in Figure 40. Unfortunately, the samples does not generate objects from ImageNet dataset. However, it also shows that they are not overfitting, because they do not show actual objects but they are quite artistic. We hypothesize that this is because the model does not have the capacity to model 1000 object classes. Hence, they stay as abstract objects.

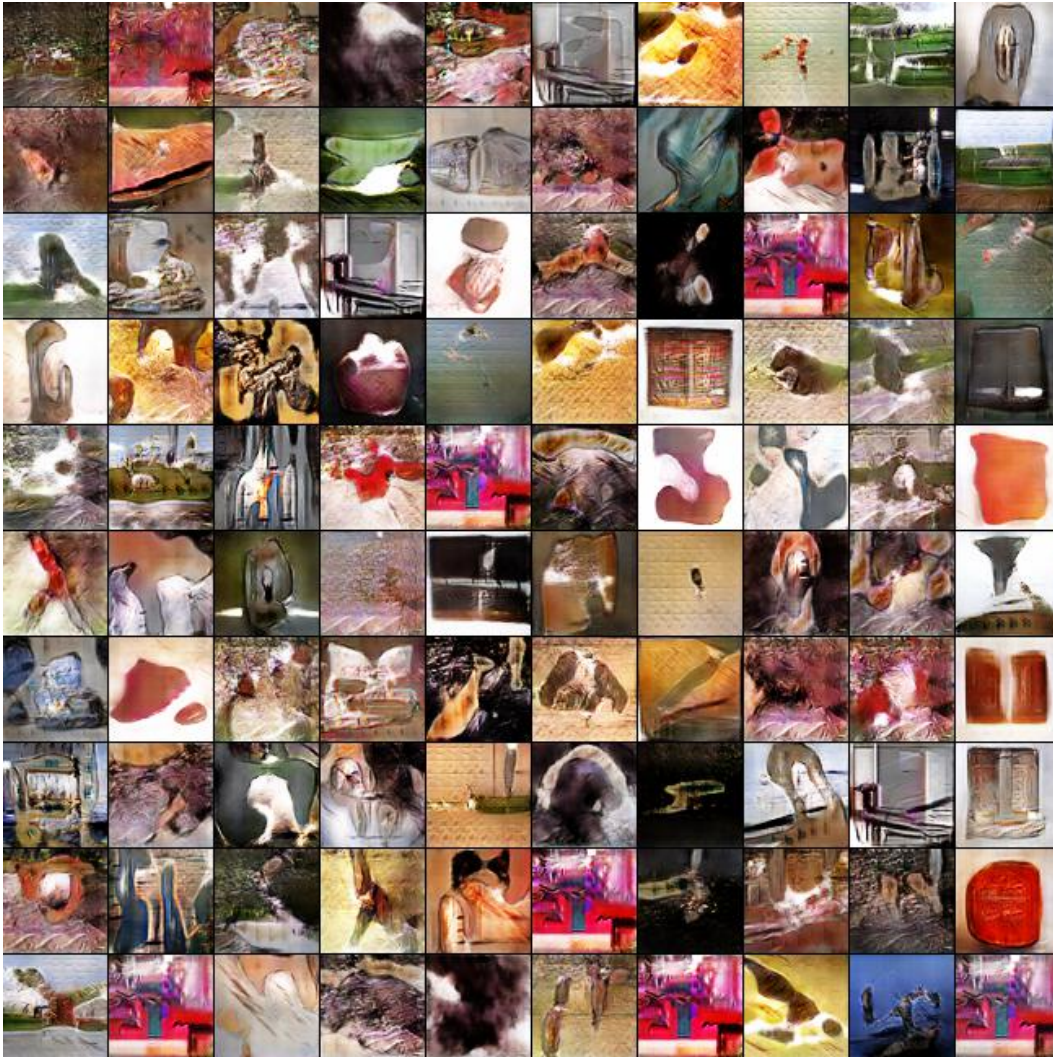


Figure 40: Samples of ImageNet images generated by GRAN3.